MOLECULAR GAS IN HIGH LUMINOSITY GALACTIC NUCLEI

Nick Scoville
Astronomy Department
California Institute of Technology

ABSTRACT. Optical and near infrared imaging of the luminous infrared galaxies show significant asymmetries, distortions, double nuclei, bars, and tidal tails indicating that the galaxies have undergone significant dynamical perturbations. Single dish CO data indicate extremely high molecular gas contents (1-20 times that of the Milky Way) in these galaxies. Approximately 25 of them have been mapped at high resolution using the millimeter interferometers and in virtually all cases, extremely high gas concentrations are found in their nuclei. In most instances, a substantial fraction of the total molecular gas content is seen within radii $\lesssim 1$ kpc; in a few cases, the gas is concentrated in a central bar or massive spiral arms (eg. NGC 1068). The dense molecular gas probably plays a pivotal role in the evolution of such dynamically disturbed systems: being dissipative, the gas can readily sink to the center of the system where it may fuel a nuclear starburst and/or build up and fuel a central active nucleus.

1. Luminous Infrared Galaxies

A spectacular result of the IRAS survey was the discovery and recognition of a class of luminous galaxies emitting the bulk of their energy at far infrared wavelengths (Soifer *et al.* 1984). Soifer *et al.* (1987) showed that the infrared luminous galaxies are the dominant population in the local universe ($z \leq 0.1$) at luminosities greater than 3×10^{11} $L_\odot$ and at luminosities greater than 10^{12} $L_\odot$, the ultraluminous IRAS galaxies outnumber optically selected quasars 2:1. The luminous infrared galaxies are also extraordinarily rich in molecular gas with H_2 masses in the range $2\text{-}50 \times 10^9$ $M_\odot$ (Sanders *et al.* 1986, 1990)—1-20 times that of the Milky Way. Although the high luminosity (10^{11}-10^{12} $L_\odot$) and ultraluminous ($\geq 10^{12}$ $L_\odot$) galaxies all have large masses of molecular gas, their gas contents are less elevated than the luminosities, relative to those of normal galaxies like the Milky Way. It is therefore clear that these objects are not simply scaled up, more massive versions, of normal spiral galaxies, but that they represent a new, perhaps transitory, phase in the evolution of galaxies.

Major questions posed by the luminous infrared galaxies are: 1) the role of large-scale galactic dynamics in determining the ISM distribution, 2) whether the high luminosity is generated by a high efficiency, short duration, starburst, or due to star formation with an initial mass function biased towards high mass stars, 3) whether there exist central non-thermal energy sources contributing significantly to the luminosity, and 4) the relationship of the luminous infrared galaxies to AGNs and QSOs. In other contributions to this symposium, the bulk molecular gas and infrared properties of these galaxies are reviewed (eg. Sanders 1990); here we concentrate on galaxies with luminosity $>10^{11}$ $L_\odot$ for which high resolution millimeter-wave aperture synthesis data have been obtained. After summarizing

F. Combes and F. Casoli (eds.), Dynamics of Galaxies and Their Molecular Cloud Distributions, 315–322.

Table 1. OVRO Observations of High Luminosity IRAS Galaxies

Object	$< cz >$ km s^{-1}	D Mpc	Radius " (kpc)	L_{IR} $10^{11}L_{\odot}$	Nuclear M_{H_2} $10^{9}M_{\odot}$	M_{H_2}/M_{dyn}	CO morphology
Mrk 231	12660	174	<3.5 (2.9)	34.7	36.0		100% nuclear source[a]
IRAS 17208 – 0014	12850	171	<1.5 (1.2)	27.0	56.0		100% nuclear source[b]
Arp 220	5452	77	1 (0.3)	15.5	16.3	0.90	70% nuclear source
VII Zw 31	16245	221	2.5 (2.7)	8.7	29.4		60% nuclear source[a]
IRAS 10173 + 0828	14680	196	3.5 (3.3)	6.0	9.0		40% nuclear source[b]
NGC 6240	7285	101	3.5 (1.7)	6.6	11.2	0.77	interacting pair[c]
IC 694 (Arp 299)	3030	42	1.3 (0.3)	4.1	3.6		triple source[d]
VV114	6028	78	2.5 (0.9)	4.2	10.0		double source[a]
NGC 1614	4847	62	2 (0.6)	4.0	6.0		30% nuclear source[a]
Arp 55	11957	163	4 (3.2)	3.9	17.3	0.6	double source[e]
NGC 1068	1137	18	1.5 (0.13)	1.5	4.5		ring+nuclear source[f]
NGC 7469 (Arp 298)	4963	66	2.5 (0.8)	2.6	7.4	0.7	30% nuclear source[e]
ZW 049.057	3900	52	1.5 (0.4)	1.7	4.0		40% nuclear source[b]
NGC 828	5359	72	2.5 (0.9)	2.1	11.8	0.31	interacting pair[e]
NGC 2146	838	21	4/13 (0.4)	1.2	4		[g]
NGC 3079	1137	24	3/7 (0.3)	0.7	5	0.2	[h]
NGC 520 (Arp 157)	2261	29	2.5 (0.4)	0.6	3.2		interacting pair[e]
NGC 4038/39 (Arp 244)	1550	21	3.5 (0.4)	0.2	0.8		triple source[i]

References: a-Scoville *et. al.* 1989; b-Planesas, Mirabel, and Sanders 1990; c-Wang, Scoville, and Sanders 1990; d-Sargent and Scoville 1990; e-Sanders *et. al.* (1988); f-Planesas, Scoville, and Myers 1990; g-Young, Claussen, and Scoville 1988; h-Young *et. al.* 1988; i-Stanford *et. al.* 1990.

https://doi.org/10.1017/S0074180900244367 Published online by Cambridge University Press

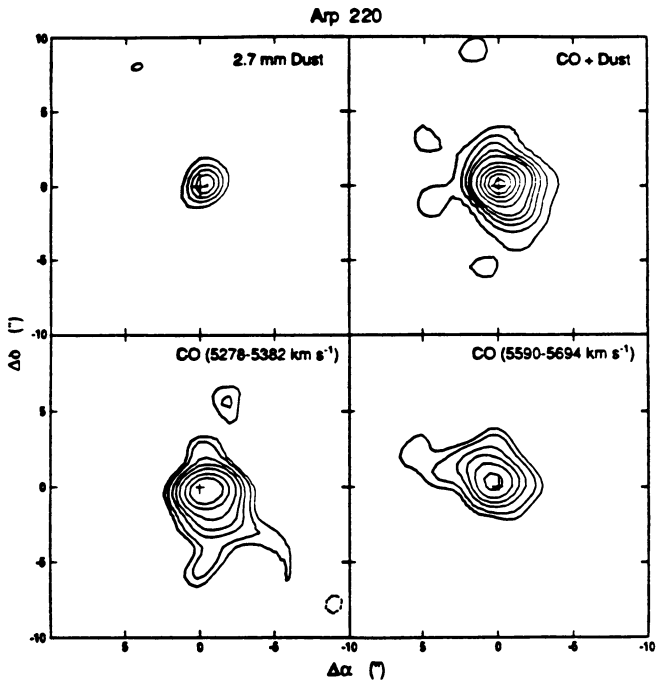

Figure 1. The λ=2.7 mm dust emission and integrated CO emission are shown in the upper panels as a function of displacement coordinates from the centimeter-wave non-thermal radio peak in Arp 220. Contours are at 8, 16, 24, 32, 40, 60, 80, 100, 120, and 140 mJy/beam. In the lower panels, the CO emission at 5278–5382 and 5590–5694 km s^{-1} are shown. Contours are at 3.1, 4.7, 7.8, 10.9, 15.6, 23.4, and 31.2 Jy km s^{-1}/beam. The synthesized beam is 1.9 x 2.1″ (PA=96°, Scoville *et al.* 1990).

the CO aperture synthesis results for these galaxies and discussing in detail new 2″ mapping in Arp 220, the prototype ultraluminous galaxy, we comment on evolutionary scenarios for these galaxies.

2. Millimeter-wave Interferometry

Approximately 25 high luminosity galaxies have now been imaged with interferometers in the 2.6 mm CO line. In Table 1, the observational results are summarized for eighteen systems observed with the Owens Valley interferometer (cf. Scoville *et al.* 1990). Seven galaxies, some of which are in the Owens Valley sample, have also been observed using the Nobeyama array (Okimura 1990) and two Seyfert galaxies have been observed using BIMA (Meixner *et al.* 1990). The spatial resolutions of these maps are 2-7″, a factor of 10 better than is possible with single dish observations.

The galaxies listed in Table 1 span the luminosity range 2×10^{10}-3×10^{12} $L_\odot$ (λ=8-1000 μm) and the masses of molecular gas in the nuclear sources are 10^9-4×10^{10} $M_\odot$ (assuming the Galactic CO-to-H_2 conversion factor: 3×10^{20} cm^{-3} (K km $s^{-1})^{-1}$). They all have

https://doi.org/10.1017/S0074180900244367 Published online by Cambridge University Press

infrared luminosity-to-molecular mass ratios significantly exceeding that of the Milky Way (4 $L_\odot$ $M_\odot{}^{-1}$, Scoville and Good 1989); the highest (Mrk 231) has a ratio of 200 $L_\odot$ $M_\odot{}^{-1}$. It is also clear from Table 1 that the H_2 gas is very concentrated. In most cases, the size of the CO emitting region is $\lesssim 1$ kpc in radius. Below, we describe in detail new results for Arp 220—the prototype ultraluminous infrared galaxy.

Arp 220

Arp 220 has an infrared luminosity at λ=8-1000 μm of 1.5×10^{12} $L_\odot$, exceeding that in the visual by nearly 2 orders of magnitude and placing it in the luminosity regime of quasars. Recent single dish measurements show the CO emission extending over a velocity range of 900 km s^{-1} and the derived H_2 mass is 3.5×10^{10} $M_\odot$, approximately a factor of 15 greater than that of the Galaxy (Solomon, Radford, and Downes 1990). At optical wavelengths, the galaxy appears approximately spherical with a central dust lane and tidal tails, both characteristics of galactic merging, extending up to 70 kpc away (Sanders *et al.* 1988).

In Figure 1, the interferometric maps at 2″ resolution (750 pc) are shown from a recent Owens Valley study (Scoville *et al.* 1990). The continuum (mostly dust emission) and CO emission are shown in the upper panels as a function of displacement coordinates from the cm-wave radio continuum peak (Norris 1988). Both the CO and 110 GHz continuum peak are within 0.5″ of the western component of the nucleus seen in high resolution near infrared and radio maps (eg. Graham *et al.* 1990). In addition to the compact nuclear source, an extended CO emission component can be seen in maps with smaller velocity ranges. In the lower panels of Figure 1, the emission is shown for velocity windows (ΔV=104 km s^{-1}), centered at 5330 and 5642 km s^{-1}. The low level contours of CO emission are clearly extended along a NE-SW direction. The full velocity range of CO emission is seen in the central component, while a more limited velocity range is seen in positions offset along the extended component.

The CO emission can be separated into two components: a core 1.4x1.9″ and an extended component 7x15″ (deconvolved sizes). The former contains 2/3 of the flux detected by the interferometer; the latter contains the remaining 1/3. Comparison of the total CO line flux detected in the interferometer maps with that seen in single dish measurements made with the IRAM 30 m telescope (Solomon, Radford, and Downes 1990) indicates that these two components account for 80% of the total CO emission from Arp 220. The highest velocity emission is probably all from the core source.

For the adopted distance of 77 Mpc, the H_2 masses in the core and extended components are 1.8×10^{10} $M_\odot$ and 9×10^9 $M_\odot$ respectively (adopting the Galactic CO-to-H_2 conversion ratio). The mean diameter of the core component ($\sim$1.7″) corresponds to a radius of 315 pc and the H_2 density, smoothed out over the volume is 2900 cm^{-3}. If we assume that the full range of CO velocities (ΔV_{FWZI}=900 km s^{-1}) exists within the central source of radius 315 pc, then the dynamical mass is 2.5×10^{10} $M_\odot$ for a spherical distribution. This dynamical mass is almost precisely equal to the total gas mass (H_2+He) for the core component.

In Figure 1 (lower panels), a velocity gradient in both the core and extended components may be seen—the lower velocity emission shifted to the Southwest of the nucleus, the higher velocity emission to the Northeast. The direction of this velocity gradient is parallel to the major axes (PA=52-63°) of the two CO emission components and to the dust lane seen

prominently in optical photographs. Thus, the molecular gas has partially relaxed to a disk-like configuration with angular momentum playing a significant role in the gas distribution, probably inhibiting somewhat the further collapse towards the center.

The λ=2.7 mm continuum flux ($\sim$30 mJy) provides a significant constraint on the emission measure of ionized gas and thus the O star luminosity in the nucleus of Arp 220 (Scoville *et al.* 1990). If the maximum residual 2.7 mm flux after subtraction of the non-thermal and dust components is taken to be $\lesssim$10 mJy and it is assumed to be *entirely* free-free emission, then the upper limit for the emission rate of Lyman continuum photons is 7.5×10^{54} s^{-1}. For an O5 star (40 $M_\odot$), $Q_*=1.3\times10^{49}$ s^{-1} and the ratio of the bolometric luminosity to the ionizing photon production rate is 1.9×10^{-44} $L_\odot$ s^{+1} (Panagia 1973). The total luminosity corresponding to the derived upper limit to the ionizing photon production rate would be 1.4×10^{11} $L_\odot$ for a population of O5 stars. Early O type stars by themselves would therefore fail to provide the observed far infrared luminosity in Arp 220 by a factor of at least 10. If a starburst is to account for the luminosity , its duration must exceed 10^8 yr or the IMF must be deficient at $\gtrsim$ 30 $M_\odot$(cf. Scoville *et al.* 1990).

3. Nuclear Gas Concentrations

In Figure 2, the luminosity-to-H_2 mass ratios are shown as a function of the central gas surface density ($M_\odot$ pc^{-2}) for the galaxies listed in Table 1. Only those galaxies for which actual size measurements exist (rather than upper limits to the unresolved source size) are plotted. Figure 2 clearly shows a trend for increasing luminosity-to-mass ratios with increasing central gas surface densities. These data thus strongly support the hypothesis that the high "efficiencies" of energy generation (L_{IR}/M_{H_2}) seen in the infrared galaxy nuclei must be linked to the high central gas concentrations.

There exists three basic classes of models proposed to account for the high luminosities of these galaxies: the kinetic energy liberated during the collision of the interstellar media in merging galaxies (Harwit *et al.* 1986), nuclear starbursts (eg. Joeseph, Wright, and Wade 1984), and a dust embedded active nucleus (eg. Sanders *et al.* 1988). Starburst models have two flavors—the formation of stars with a higher efficiency per unit mass of interstellar gas or with an initial mass function more heavily weighted towards high mass stars than in the Milky Way. In the Galaxy, it has been suggested that high mass star formation is triggered by the expansion of HII regions or supernova shells (eg. Elmegreen and Lada 1977) or by cloud-cloud collisions (Scoville, Sanders, and Clemens 1986). Both processes depend on the *concentration* of molecular gas, not merely the total H_2 mass. The correlation seen in Figure 1 between the luminosity-to-mass ratios and the central gas surface densities is consistent with all three classes of energy generation—the dissipation of kinetic energy will occur more rapidly in a dense gas configuration, the formation of high mass stars via stimulated or binary processes (such as cloud-cloud collisions) will occur more rapidly when the gas is concentrated, and the accretion rate onto a compact, central black hole should in principle increase with increasing ISM density.

Virtually all of the infrared luminous galaxies show evidence of significant dynamical perturbations due to a central stellar bar or galactic interaction (cf. Sanders 1990). The interstellar matter can play a central role in the dynamics for both cases inasmuch as it is dissipative and the gas will respond irreversibly to the perturbation, in general sinking

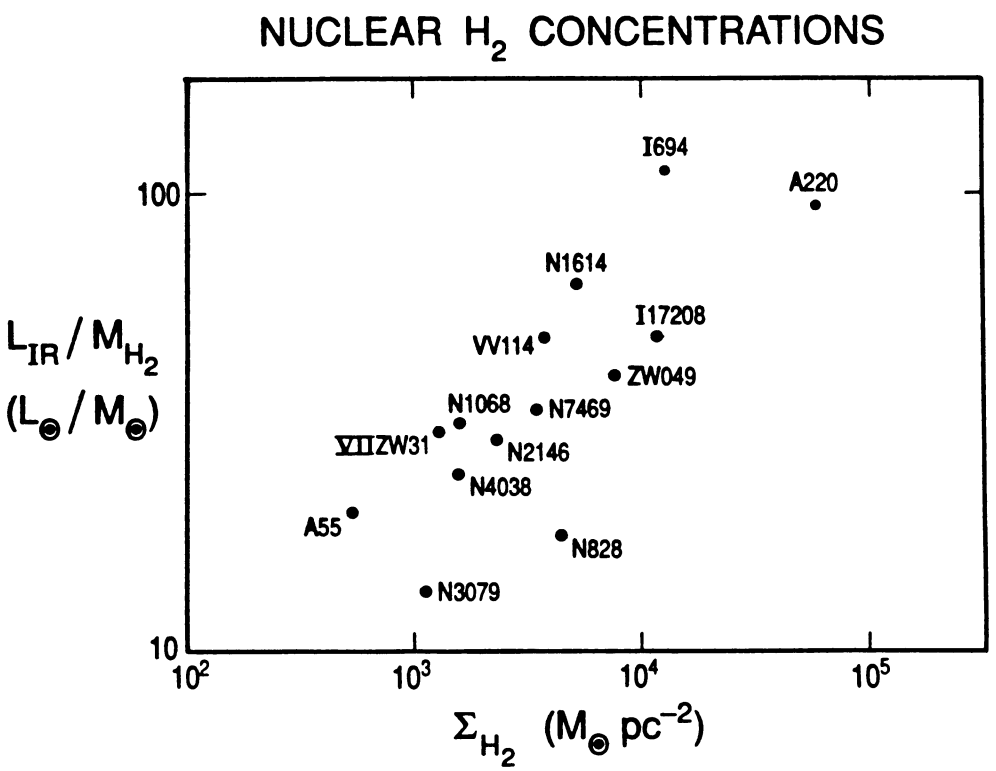

Figure 2. The infrared luminosity-to-molecular gas mass ratios are shown as a function of the central gas surface density in 14 luminous infrared galaxies (Table 1). A general correlation is seen with increasing luminosity-to-mass ratios being found in the galaxies with higher gas surface densities. In computing the luminosity-to-mass ratios, the total infrared luminosity was attributed to the nuclear source since the IRAS data have insufficient resolution to separate out any extended component. For NGC 1068, only the far-infrared and molecular gas components associated with the spiral arms at 10-15″ radius are used (cf. Planesas, Scoville, and Myers 1990).

towards the center of the potential well. The H_2 masses for the luminous infrared galaxies are large but in most cases, not more than would be found in *two* galaxies such as M51 ($M_{H_2} \sim 10^{10}$ $M_\odot$, Scoville and Young 1983). [Notable exceptions are the highest luminosity systems, VII Zw 31, Arp 220 and Mrk 231 for which the H_2 masses are $2\text{-}5 \times 10^{10}$ $M_\odot$.] Thus, in most cases, it is plausible that the luminous infrared galaxies result from the merging of two gas-rich spiral galaxies and that the disturbed dynamics in the merging system results in dissipation of kinetic energy (and outward transport of angular momentum) in the ISM, leading to the deposition of a significant fraction of the original interstellar matter in the central region of the system.

https://doi.org/10.1017/S0074180900244367 Published online by Cambridge University Press

Given the highly concentrated distribution of the interstellar gas and the high luminosity energy densities it is unlikely that the molecular gas is arranged in GMCs similar to those containing the bulk of the Galactic H_2. It is to be expected that both the mean gas density and gas temperatures will be considerably higher and these in turn will affect the rate of emission of CO line photons per unit mass of molecular hydrogen. The CO-to-H_2 conversion ratio (α) scales approximately as $\rho^{1/2}/T_X$ (cf. Scoville and Sanders 1987). To some extent, the elevated gas densities and temperatures will have cancelling effects on the CO-to-H_2 conversion ratio. For example, in Arp 220, the mean gas density, assuming the central H_2 mass is smoothed out over a volume 315 pc in radius is 2900 cm^{-3}. If the gas temperature is 45 K (the far infrared color temperature) and n_{H_2}=2900 cm^{-3}, then the $\rho^{1/2}/T$ scaling reduces the CO-to-H_2 conversion ratio by a factor of 2. Somewhat higher volume densities (10^4-10^5 cm^{-3}) are deduced by Solomon, Radford, and Downes (1990) on the basis of CS line measurements. In summary, the H_2 mass estimates, based on the CO and CS emission, are somewhat uncertain, but probably not by a large factor.

In Table 1, the gas mass fraction (M_{H_2}/M_{dyn}) is given for those galaxies in which the nuclear mass concentration is well resolved and for which the velocity dispersion can be estimated using the CO line-width. For the six cases where this ratio has been evaluated, it is in the range 0.2-0.9, indicating that a significant fraction of the total mass is contained in interstellar gas. Such high gas mass fractions may reflect the inappropriateness of using the galactic CO-to-H_2 conversion factor. On the other hand, it is also possible that the gas does indeed constitute a large fraction of the overall mass since numerical simulations of merging galaxies (Hernquist 1989) which include a gas component show that due to its dissipative nature, the gas sinks to the center of the merged system more readily than the stellar component. Thus, it is to be anticipated that during the evolution of a merging galaxy system, there will be regions with very large gas mass fractions.

4. Evolutionary Scenarios

Based on the studies described above, three generalities can be drawn for the highest luminosity infrared galaxies: essentially all show optical morphologies indicative of a recent galactic interaction or merging, they have abundant molecular gas with total H_2 masses 1-20 times that of the Milky Way, and most show extremely high concentrations of gas in their nuclear regions. These facts strongly indicate that the onset of the ultraluminous phase is triggered by a strong galactic interaction and that the molecular gas plays a pivotal role in producing the high infrared luminosities. The gas, being highly dissipative, accumulates in the center of the merged galaxy system. The high concentration of molecular gas in the nucleus can then lead to a runaway burst of star formation as a result of stimulated effects or the compression of interstellar clouds as a result of cloud-cloud collisions. Norman and Scoville (1988) suggest that the formation of a dense young stellar cluster at the nucleus can naturally lead to the buildup of a massive black hole if the potential well is sufficiently deep to trap the stellar mass loss material. On the other hand, if the burst of star formation is spread out, the high mass stars may ionize and disperse the interstellar gas. The identification of galaxies and AGNs in this post-IRAS phase with a bare starburst nucleus should be an important goal of future research.

Acknowledgement

This research is supported in part by NSF Grant AST 87-14405. It is a pleasure to thank my collaborators in this work (C. Norman, P. Planesas, D. Sanders, A. Sargent, T. Soifer, and Z. Wang).

5. References

Elmegreen, B.G. and Lada, C.J. 1977, *Ap. J.*, **214**, 725.

Graham, J.R., Carico, D.P., Matthews, K., Neugebauer, G., Soifer, B.T., and Wilson, T.D. 1990, *Ap. J. (Letters)*, **354**, L5.

Harwit, M., Houck, J.R., Soifer, B.T., and Palumbo, G.G.C. 1986, *Ap. J.*, **315**, 28.

Hernquist, L. 1989, *Nature*, **340**, 687.

Joseph, R.D., Wright, G.S., and Wade, R. 1984, *Nature*, **311**, 132.

Meixner, M., Puchalsky, Blitz, L., Wright, M., and Heckman, T. 1990, *Ap. J.*, **354**, 158.

Norman, C.A. and Scoville, N.Z. 1988, *Ap. J.*, **332**, 124.

Norris, R.P. 1988, *M.N.R.A.S.*, **230**, 345.

Okimura, S.K. 1990, IAU Symposium No. 146, "Galaxies and Molecular Cloud Distribution" ed. F. Combes (Dordrecht: Kluwer).

Panagia, N. 1973, *A.J.*, **78**, 929.

Planesas, P., Mirabel, I.F., and Sanders, D.B. 1990, *Ap. J.*(in press).

Planesas, P., Scoville, N.Z., and Myers, S.T. 1990, *Ap. J.*, (submitted).

Sanders, D.B. 1990, *IAU Symposium No. 146 "Dynamics of Galaxies and Molecular Clouds Distribution"*, ed. F. Combes (Dordrecht: Kluwer).

Sanders, D.B., Scoville, N.Z., and Soifer, B.T. 1990, *Ap. J.*, (in press).

Sanders, D.B., Scoville, N.Z., Sargent, A.I., and Soifer, B.T. 1988, *Ap. J. (Letters)*, **324**, L55.

Sanders, D.B., Scoville, N.Z., Young, J.S., Soifer, B.T., Schloerb, F.P., Rice, W.L., and Danielson, G.E. 1986, *Ap. J. (Letters)*, **305**, L45.

Sanders, D.B., Soifer, B.T., Elias, J.H., Madore, B.F., Matthews, K., Neugebauer, G., and Scoville, N.Z. 1988, *Ap. J.*, **325**, 74.

Sargent, A.I. and Scoville, N.Z. 1990 (in preparation).

Scoville, N.Z. and Good, J.C. 1989, *Ap. J.*, **339**, 149.

Scoville, N.Z. and Sanders, D.B. 1987, in *Interstellar Processes*, ed. D.J. Hollenbach and H.A. Thronson (Dordrecht: Reidel), p. 21.

Scoville, N.Z. and Young, J.S. 1983, *Ap. J.*, **265**, 148.

Scoville, N.Z., Sanders, D.B., and Clemens, D.P. 1986, *Ap. J. (Letters)*, **310**, L77.

Scoville, N.Z., Sanders, D.B., Sargent, A.I., Soifer, B.T., and Tinney, C.G. 1989, *Ap. J. (Letters)*, **345**, L25.

Soifer, B.T., Helou, G., Lonsdale, C.J., Neugebauer, G., Hacking, G., Houck, J.R., Low, F.J., Rice, W., and Rowan-Robinson, M. 1984, *Ap. J. (Letters)*, **283**, L1.

Soifer, B.T., Sanders, D.B., Madore, B.F., Neugebauer, G., Danielson, G.E., Elias, J.H., Lonsdale, C.J., and Rice, W.L. 1987, *Ap. J.*, **320**, 238.

Solomon, P.M., Radford, S.J.E., and Downes, D. 1990, *Ap. J. (Letters)*, **348**, L53.

Stanford, S.A., Sargent, A.I., Sanders, D.B., and Scoville, N.Z. 1990, *Ap. J.*, **349**, 492.

Wang, Z., Scoville, N.Z., and Sanders, D.B. 1990, *Ap. J.*, (submitted).

Young, J.S., Claussen, M.J., and Scoville, N.Z. 1988, *Ap. J.*, **324**, 115.

Young, J.S., Claussen, M.J., Kleinmann, S.G., Rubin, V.C., and Scoville, N.Z. 1988, *Ap. J. (Letters)*, **331**, L81.